Astron. Astrophys. 271, 36–50 (1993)

ASTRONOMY AND ASTROPHYSICS

Vertical magnetic fields above the discs of spiral galaxies

A. Brandenburg[1,2], K. J. Donner[3], D. Moss[4], A. Shukurov[5], D. D. Sokoloff[2,6], and I. Tuominen[3]

[1] NORDITA, Blegdamsvej 17, DK-2100 Copenhagen Ø, Denmark
[2] Isaac Newton Institute, 20 Clarkson Road, Cambridge CB3 0EH, UK
[3] Observatory and Astrophysics Laboratory, University of Helsinki, Tähtitorninmäki, SF-00130 Helsinki, Finland
[4] Mathematics Department, The University, Manchester M13 9PL, UK
[5] Computing Centre, Moscow University, Moscow 119899, Russia
[6] Department of Physics, Moscow University, Moscow 119899, Russia

Received October 21, accepted December 5, 1992

Abstract. We investigate the magnetic fields above the discs of spiral galaxies in the framework of axisymmetric nonlinear mean-field dynamo models for a disc surrounded by a spherical halo, using realistic rotation curves. We consider, in particular, NGC 4631 and NGC 891, and include turbulent diamagnetism, an anisotropy of the α effect and a galactic wind. In these models magnetic field is generated in a disc of scale height 1.5 kpc and distorted by the wind in the halo. For typical wind velocities of 50...200 km/s in the halo we find good qualitative agreement between the observed polarisation maps and those synthesised from the magnetic fields of our models: Poloidal synthesised fields dominate in the halo of NGC 4631, and horizontal fields in that of NGC 891. In some cases, a galactic wind can enhance dynamo action, contrary to previous expectations. Our results indicate that turbulent diamagnetism plays an important rôle in galactic dynamos.

Key words: galaxies – magnetic fields – hydromagnetics – NGC 4631 – NGC 891

1. Introduction

Polarisation measurements of synchrotron emission in some edge-on spiral galaxies have recently provided direct information on the magnetic fields in their halos. The most detailed observations to date are for the galaxies NGC 891, NGC 4631 and NGC 4565. In NGC 4631 (Hummel et al. 1988, 1991b; Golla & Hummel 1992) the field vectors are more-or-less radial and extend to a considerable distance from the disc plane; see Fig. 1. On small scales, however, there can be substantial deviations from the average field orientation; see Golla & Hummel (1992). (The direction of the magnetic field vectors is not known as yet, so it is impossible to say whether the field is symmetric or antisymmetric with respect to the equatorial plane. No firm conclusions can be drawn about the field orientation *in* the disc, because even for 3.5 cm waves the radio emission is almost completely depolarised (Golla & Hummel 1992).) On the other hand, in NGC 4565 the polarised emission is more strongly confined to the disc plane, and the field vectors are more or less parallel to the disc (Sukumar & Allen 1991). NGC 891 appears to be intermediate in this respect (Hummel et al. 1991b; Sukumar & Allen 1991); see Fig. 2.

There are several possible explanations for the origin of these fields. Sokoloff & Shukurov (1990) argue that such magnetic fields could be generated directly by a mean-field dynamo in the halos of these galaxies. In general this type of model should lead to large toroidal fields in the halo but, as shown in Brandenburg et al. (1992, hereafter referred to as Paper I), magnetic fields in a two-component dynamo system consisting of the disc and the halo can have quite complicated and diverse configurations. These may depend on such factors as the relative rôles of the disc and the halo in the field regeneration, and even the initial conditions (since the global dynamo time scale may be of the order of the galactic lifetime). Additionally, if there is a significant oscillating field component in the halo, the field configuration can vary markedly with phase.

The dominance of the vertical magnetic field above the galactic disc at first sight seems to be hardly compatible with galactic dynamo theory, because galactic dynamo solutions naturally have a dominant toroidal magnetic field. This feature is typical of $\alpha\Omega$ dynamos with strong differential rotation, and agrees with observations of magnetic fields in the discs of the Milky Way and nearby spiral galaxies (see e.g. Ruzmaikin et al. 1988; Chap. 7). Thus, the dominance of the vertical magnetic field in the halo of NGC 4631 implies that conventional galactic dynamo models need some modification. Elstner et al. (1992) propose that an axisymmetric dipole field (A0 mode) can explain vertical fields in NGC 4631, although this mode is less readily excited than the axisymmetric quadrupole field (S0 mode). In this paper we show that the effects associated

Send offprint requests to: D. Moss

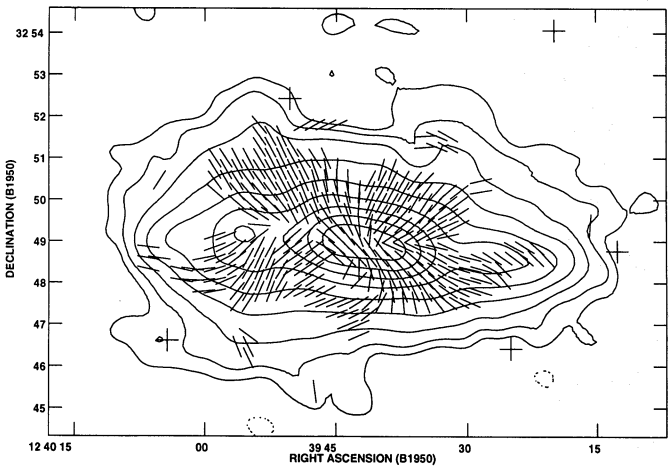

Fig. 1. Total intensity contours with magnetic field orientations indicated by vectors according to observations of NGC 4631 at 6.2 cm by Golla & Hummel (1992). The contours start at 100 mJ/beam and the interval is a factor of 2. The noise in the total intensity map is about 28 μJ/beam. Vectors are plotted only if the polarised intensity exceeds $\sim$ 70 μJ/beam). The half power beam width (HPBW) is 40″. Assuming a distance of 7.5 Mpc the scale is 1′ = 2.2 kpc

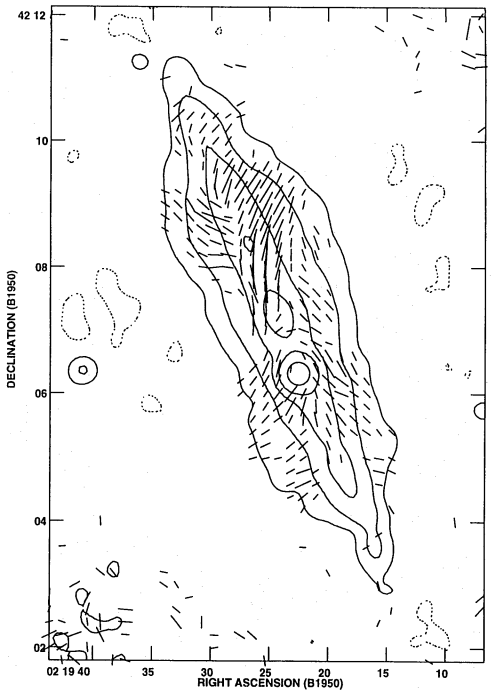

Fig. 2. Total intensity contours with magnetic field orientations indicated by vectors according to observations of NGC 891 at 6.2 cm by Sukumar & Allen (1991). The contours start at 150 μJ/beam and the interval is a factor of 4. The noise in the total intensity map is about 25 μJ/beam. Vectors are plotted only if the polarised intensity exceeds 3.5 σ ($\sim$ 50 μJ/beam). The HPBW is 40″. (The brightest source in the disc is the supernova SN1986J and not the nucleus of the galaxy!) Assuming a distance of 7.2 Mpc the scale is 1′ = 2.1 kpc

with galactic winds can lead to field configurations compatible with the observations of NGC 4631. In NGC 891 the effects of a galactic wind are relatively weak and the field orientation is more nearly horizontal, in agreement with conventional dynamo models. It is important that the strikingly different magnetic field patterns in these two galaxies can be produced by a single dynamo model by incorporating the observed rotation curves.

A second possibility has been proposed by Donner & Brandenburg (1990a), who present results for the marginal modes in models with a high-conductivity halo. These modes have a strong toroidal field confined to the disc, and a poloidal field extending into the halo. In these models the field generation was confined to a thin disc. These models again have the drawback that there is little observational support for a halo with the required properties, because the effective (turbulent) conductivity is probably lower in the halo than in the disc (Sokoloff & Shukurov 1990).

Small scale outflows of hot gas from the galactic disc, associated with galactic fountains, chimneys and Parker instabilities, can carry magnetic fields away from the disc, producing vertical magnetic fields with alternating directions at a height of a few kpc above the disc. In this case the mean field above the disc is expected to be vanishing, but polarisation planes of synchrotron emission still will show a large degree of alignment and order. However, the ordered polarisation pattern observed in NGC 4631 can hardly be explained by a chaotic magnetic field of this kind. Recent multifrequency observations of NGC 4631 by Golla & Hummel (1992) reveal a considerable Faraday rotation measure up to ± 10 rad/m^2, in some regions of the halo of this galaxy. This is direct evidence of a *regular* magnetic field in the halo of this galaxy. For an electron number density of 10^{-3}cm^{-3} and a path length of 10 kpc, this Faraday rotation measure corresponds to a longitudinal magnetic field, averaged along the line of sight, of approximately 1 μG. This value for the line of sight components of $\boldsymbol{B}$ is somewhat smaller than the total field component which is close to the equipartition value in the halo ($\approx 5\mu$ G, cf. Hummel et al. 1991b).

It has also been proposed that a galactic wind might carry the fields away from the disc where they are generated. In particular, for NGC 4631 the variation of the spectral index with height seems to indicate the presence of a wind (Sukumar & Velusamy 1985; Werner 1988). Hummel & Dettmar (1990) estimate a wind or large scale velocity of 150 km/s. We should note, however, that simple advection of field from the disc, where the toroidal field dominates, by an axisymmetric wind cannot lead to a dominance of the vertical field higher in the halo. Thus, when including the effects of a galactic wind in galactic dynamo models, we expect the more fundamental changes to be associated with the presence of velocity shear in the dynamo system.

The models we shall consider in this paper are based on the recent realisation that in the Milky Way a thick disc is also observed both in the warm neutral gas (Lockman et al. 1986) and in the warm ionised gas (Reynolds 1989; Cordes et al. 1991), in addition to the thin, denser, gas disc. A similar thick ionised disc

has also been detected in NGC 891 (Rand et al. 1990; Dettmar 1990). Our view of the intercloud medium is along the lines proposed by Cox (1990), i.e. we consider the neutral and ionised gas as a single dynamical component forming a thick turbulent disc. The turbulence is maintained by the energy input from star formation in the thin disc, and possibly by Rayleigh-Taylor-Parker type instabilities, although the detailed mechanisms of maintenance and support are still unclear (Boulares & Cox 1990; Lockman & Gehman 1991; Ko et al. 1991). It is a natural consequence of this type of model, which also includes a hot interstellar gas component, that the gas flow may go over into a galactic wind (see e.g. Habe & Ikeuchi 1980).

In this paper we focus on the effects of a wind on galactic dynamos, and in particular its efficiency in making the halo field more nearly radial. The dynamo can be operative only provided that the galactic wind is not so strong as to advect magnetic fields away before they are amplified by the dynamo. A naive upper limit on the admissible galactic wind speed W is given by

$$W = \frac{R}{\tau} \approx 15\,\mathrm{km/s}, \tag{1}$$

where $R \approx 15$ kpc is the halo radius and $\tau \approx 10^9$ years is a typical growth time for the halo magnetic field. Such a kinematic estimate would indicate that a rather weak galactic wind might significantly affect and even suppress dynamo action. However, we show below that in the outer parts of the halo much larger wind velocities (50...200 km/s) can still be tolerated by a dynamo.

The interplay between the wind flow and the regular magnetic field can also be clarified by the following simple arguments. With a typical particle density in the halo of about $10^{-3}\mathrm{cm}^{-3}$, and assuming a typical wind speed of about $W = 100$ km/s, we find the kinetic energy density to be of the order $10^{-13}\mathrm{g\,cm^{-1}\,s^{-2}}$. With $|\boldsymbol{B}| = 1\,\mu$G we obtain typical values for the magnetic energy density of the same order of magnitude, so the magnetic field could then significantly modify the wind. However, the strength of the interaction will depend on both the magnetic field and wind geometries: for example it will be ineffective when the magnetic field and velocity vectors are approximately parallel. It would be a major task to solve self-consistently equations describing the magnetic field evolution together with the momentum equation governing the rotation law and the generation of galactic wind. Instead, we here restrict ourselves to a simple quasi-kinematic alpha-quenched model, that allows us to estimate the wind strength that is still compatible with dynamo action, and to investigate the consequences in terms of observable polarisation maps. It should be kept in mind, however, that in a fully dynamical calculation the field might turn out to be strong enough to modify significantly the wind.

In most cases we discuss models with fields of S0 configuration, as these are the most stable solutions (cf. Paper I). We postpone a thorough discussion of more complex field structures to a future paper (see, however, Sect. 5.7). Even though our models are based on the observed rotation curves of NGC 4631 and NGC 891, we have not attempted to reproduce all the observed details of the magnetic fields of these galaxies. Rather we have investigated their general properties, and reasons for the dominance of poloidal or toroidal fields in galactic halos. In order to facilitate comparisons with observations we present our results in the form of synthetic maps of the total and polarised synchrotron emission.

2. The model

The evolution of the average magnetic field $\boldsymbol{B}$ is governed by the mean-field dynamo equation

$$\frac{\partial \boldsymbol{B}}{\partial t} = \mathrm{curl}\,(\boldsymbol{u} \times \boldsymbol{B} + \mathscr{E}), \quad \mathrm{div}\,\boldsymbol{B} = 0, \tag{2}$$

(e.g. Krause & Rädler 1980), where $\boldsymbol{u} = \hat{\boldsymbol{\phi}}\varpi\Omega + \boldsymbol{u}_p$. Ω is the angular velocity and the poloidal velocity component $\boldsymbol{u}_p$ is the galactic wind. Here we use spherical polar coordinates r, θ, ϕ, with $\varpi = r\sin\theta$ the distance from the rotation axis and $z = r\cos\theta$ the height above the galactic plane. The effects of the small scale velocity and magnetic fields are included into the turbulent electromotive force

$$\mathscr{E} = \alpha(\boldsymbol{B} + \alpha_z B_z \hat{\boldsymbol{z}}) + \boldsymbol{\gamma} \times \boldsymbol{B} - \eta\,\mathrm{curl}\,\boldsymbol{B} + \ldots \tag{3}$$

The $\alpha\boldsymbol{B}$ and η curl $\boldsymbol{B}$ terms on the right hand side of Eq. (3) represent the standard isotropic α effect and the turbulent magnetic diffusion, where η is the turbulent magnetic diffusivity, assumed to be isotropic. The α_z and $\boldsymbol{\gamma}$ terms are anisotropic contributions to the symmetric and antisymmetric parts respectively of the full α tensor. Below we refer to models with anisotropic α if α_z is nonzero. The dots in Eq. (3) denote further anisotropic contributions (e.g. Krause & Rädler 1980), which are here assumed to be less important.

The value of α_z is model dependent and can vary between +10 (Rüdiger 1990) and −4 (Brandenburg et al. 1990). A negative value of α_z has also been obtained recently by Ferrière (1992) and Rüdiger & Kichatinov (1993). Meinel et al. (1990) have stressed the possible importance of this term for explaining the generation of nonaxisymmetric fields in galaxies.

The $\boldsymbol{\gamma}$ term corresponds to a turbulent diamagnetism with

$$\boldsymbol{\gamma} = -\tfrac{1}{2}\boldsymbol{\nabla}\eta \tag{4}$$

(Vainshtein & Zeldovich 1972; Roberts & Soward 1975). This term leads to a transport of magnetic field in the direction of decreasing magnetic diffusivity which, in our case, is towards the galactic plane. Thus, it can counteract the effect of a galactic wind in the immediate vicinity of the disc.

Equation (2) is solved on a r, θ mesh with 41×41 equally spaced mesh points in one quadrant of a meridional plane, in a region with radius R. We take a standard value for R of 15 kpc. In some cases we checked the accuracy using 63×64 mesh points, but a resolution of 41×41 mesh points was generally sufficient. We employ a DuFort-Frankel scheme for the diffusive terms and second or fourth order (cubic splines) finite differences for the explicit terms. The maximal time step is determined empirically by accuracy requirements and is typically around 2×10^{-5}. See Paper I for further details.

2.1. Magnetic diffusivity

The turbulent magnetic diffusivity may be estimated by $\eta \approx \frac{1}{3}u_t\ell$, where u_t is the rms velocity of the turbulence and ℓ the correlation length. In Paper I we used $u_t \approx 100$ km/s, $\ell \approx 500$ pc for the halo, and $u_t \approx 10$ km/s, $\ell \approx 100$ pc at $z = 0$. We approximate this spatial variation by a Gaussian profile of the form

$$\eta(z) = \eta_0 \left[1 - \eta_1 \, e^{-(z/h)^2}\right], \tag{5}$$

where $0 < \eta_1 < 1$ for a turbulent diffusivity that is larger in the halo than in the disc, and h is the half-width of the disc. In all the cases reported below we use $\eta_1 = 0.95$ and $h = 0.1R$ (= 1.5 kpc for the thick disc, or Reynolds layer); see the left hand panel of Fig. 3.

We should note that we do not explicitly include here the thinner, dense, galactic disc that is often considered in "thin disc" dynamo models for spiral galaxies. Thus we assume that the large scale properties of the magnetic field at heights exceeding several kpc above the midplane are not strongly affected by the thin disc. With considerably better spatial resolution it would be possible to include such a thin disc, but this would also require shorter time steps and the large amount of cpu-time then needed would make it very difficult to investigate a reasonable range of models. We should also note that a higher resolution can sometimes lead to unexpected numerical instabilities (cf. Krasheninnikova et al. 1990). Ideally, one would also adopt values of η_1 somewhat closer to unity, but this would also require better resolution. Progress could be made by using a nonuniform mesh that is denser near the disc plane.

2.2. Rotation law

For the angular velocity Ω we use a modified Brandt curve

$$\Omega(\varpi, z) = \Omega_0 f(z) \left[1 + \left(f(z)\frac{\varpi}{\varpi_\Omega}\right)^n\right]^{-1/n}, \tag{6}$$

where the factor $f(z) = \exp(-|z|/z_\Omega)$ has been included to simulate a decrease of Ω with distance from the disc plane. (The jump in the gradient at $z = 0$ was removed in the numerical computations.) The rotational velocity as $\varpi \to \infty$ is $V_0 = \Omega_0\varpi_\Omega$. In the following we use $n = 3$. In all cases considered below the qualitative behaviour of the solution did not depend crucially on whether or not the $f(z)$ factor was included, provided z_Ω is at least a few kpc. The strength of the Ω effect is specified by the dimensionless parameter $C_\Omega = \Omega_0 R^2/\eta_0$, which can also be written as

$$C_\Omega = \frac{V_0 R}{\eta_0}\frac{R}{\varpi_\Omega}. \tag{7}$$

The rotation curves of NGC 891 and NGC 4631 are qualitatively similar, with a central rigidly rotating part and an outer flat part, with $V_0 = 150$ km/s, $\varpi_\Omega = 0.1R$ for NGC 4631 (Weliachew et al. 1978) and $V_0 = 225$ km/s, $\varpi_\Omega = 0.2R$ for NGC 891 (Sancisi & Allen 1979; Rupen 1991). This gives $C_\Omega = 1400$ for NGC 4631 and $C_\Omega = 1040$ for NGC 891. According to recent measurements of the rotation curve of NGC 4631 the value of ϖ_Ω is perhaps nearer $0.15R$ (Golla 1992). For comparison we use this value in one of the models below.

2.3. The α effect

The α effect is taken in the form

$$\alpha(\varpi, z, t) = \frac{\Omega(\varpi, z)\ell^2/h}{1 + \alpha_B \boldsymbol{B}^2(\varpi, z, t)}\sqrt{2}\frac{z}{h}e^{1/2-(z/h)^2}. \tag{8}$$

We also define a dimensionless parameter $\xi \approx \ell^2/(hR)$. Expression (8) is based on the well known formula $\alpha \sim -\ell^2\boldsymbol{\Omega}\cdot\boldsymbol{\nabla}\ln(\rho u_t)$ (Krause 1967), and numerical factors are introduced for normalisation. With $\ell = 100...500$ pc we have $\xi = 4\,10^{-4}...10^{-2}$. However, the adopted expressions of α and η should be regarded as order of magnitude estimates, and we shall therefore treat ξ as a free parameter that we choose large enough to excite the dynamo. In most of the cases reported below we used $\xi = 0.02$.

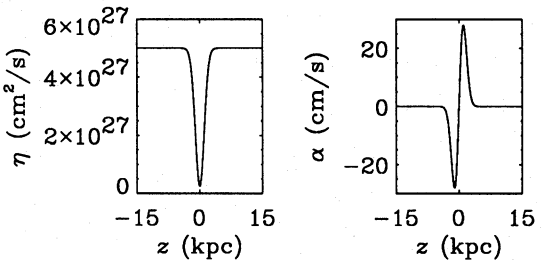

Fig. 3. The adopted vertical profiles of η and α along the rotation axis for $C_\alpha = 1400$, $\xi = 0.02$, and $\boldsymbol{B} = \boldsymbol{0}$

The dynamical feedback onto the turbulence is determined by the coefficient

$$\alpha_B = k(\mu_0\rho u_t^2)^{-1}, \tag{9}$$

where k is dimensionless and of order unity. The spatial variation of α_B between disc and halo is not very large, because ρ and u_t^2 vary roughly in inverse proportion to one another. Thus, we consider here α_B to be constant, and k is a constant of order unity. Its value is determined by the details of the interaction between the magnetic field and the turbulence.

The adopted profile for α is displayed in the right hand panel of Fig. 3. Note that, unlike the models discussed in Paper I, α differs significantly from zero only within the disc, $|z| < h$. When α is relatively large in the halo, the magnetic field distributions computed here always have a dominant toroidal component. Thus, the magnetic field pattern observed in NGC 4631 indicates a small α effect in the halo whilst NGC 891 and NGC 4565 are compatible with stronger dynamo action in the halo.

2.4. Galactic wind

In most of our models we include a galactic wind, described by a poloidal velocity field, $\boldsymbol{u}_p$. At large distances from the galactic plane, the wind velocity becomes more nearly radial; this approximation is natural when considering the outer parts of the halo. It is clear that near the disc the wind flow has an approximate cylindrical symmetry (cf. Habe & Ikeuchi 1980), since the wind flow originates in the galactic disc as a hot gas rising above the disc. (For recent galactic wind models see Breitschwerdt et al. 1991, and references therein.) As long as the distribution of supernovae, which are the source of the hot gas, terminates at $\varpi \simeq 15$ kpc in the disc of the Milky Way, this radius is taken as the outer boundary of the wind outflow in the disc. Since the radial scale of the total mass distribution in galactic discs is typically about 4 kpc, we assume that the wind flow is transformed from cylindrical symmetry to spherical at a comparable height. Thus, we adopt the form

$$\boldsymbol{u}_p = W_r \frac{\boldsymbol{r}}{R}\left[1 - w_1 e^{-(z/z_W)^2}\right] \tag{10}$$

$$+ W_z \frac{\boldsymbol{z}}{Z_W} \frac{27}{4} \frac{\varpi^2(R-\varpi)}{R^3} \sqrt{2} e^{1/2-(z/Z_W)^2} \tag{11}$$

for the wind velocity field. The numerical factors in this expression ensure that the maxima of the coefficients of W_r and W_z are unity. The radial dependence of the vertical velocity in the disc (second term in Eq. (11)) is chosen to have a mild maximum near $\varpi = 10$ kpc. Since the radial wind should not blow through the disc we have introduced a gaussian truncation with scale z_W and amplitude $w_1 = 1$, which gives a smooth transition from cylindrical to spherical geometry at $z \approx z_W$. For all models we assume $z_W = Z_W = 0.2R$ corresponding to 3 kpc, if $R = 15$ kpc is assumed. Examples of the wind velocity fields adopted are illustrated in Fig. 4. We often characterise the wind strength by reference to the value of W_r. We should stress that this is a measure of the wind velocity at the *outer* boundary of the halo.

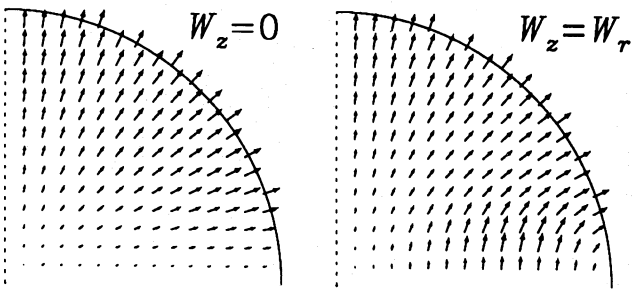

Fig. 4. Geometry of the wind velocity field in a meridional plane for $W_z = 0$ (left hand side) and $W_z = W_r$ (right hand side). The dotted line on the left hand side corresponds to the rotation axis

2.5. Boundary conditions

In the case of vanishing wind velocity we adopt a vacuum boundary condition for the magnetic field at $r = R$. This is, however, incompatible with a nonvanishing wind velocity at the outer boundary, because it leads to an accumulation of toroidal field there. For this reason we used an "open" boundary condition, with $\partial(ra)/\partial r = \partial(rb)/\partial r = 0$ for nonvanishing wind velocities, where a is the ϕ-component of the magnetic vector potential and $b = B_\phi$. A similar boundary condition was used by Moss et al. (1990) in a different context.

2.6. Units

We introduce nondimensional quantities by, as usual, measuring r, ϖ and z in units of R, time in units of R^2/η_0 and velocities in units of $[\boldsymbol{u}] = \eta_0/R$. Since α_B is assumed to be constant we can measure the magnetic field in units of $[\boldsymbol{B}] = (\mu_0 \rho u_t^2/k)^{1/2}_{\rm disc}$, where k is defined in Eq. (9). With $R = 15$ kpc, $\eta_0 = 5\,10^{27}$ cm^2/s, $\rho_{\rm disc} = 2\,10^{-24}$ g/cm^3, we have $[\boldsymbol{u}] \approx 1$ km/s and $[\boldsymbol{B}] \approx 5\,\mu{\rm G}/k^{1/2}$.

3. Polarised synchrotron emission

The intensity I of the synchrotron radiation is obtained by integrating the emissivity ε through the galaxy, i.e.

$$I = \int_{-\infty}^{\infty} \varepsilon ds. \tag{12}$$

Here we take, in gaussian cgs units,

$$\varepsilon = 0.933\,10^{-23} c(\gamma)\, K\, |\boldsymbol{B}_\perp|^{(\gamma+1)/2} \left(\frac{\nu}{6.26\,10^{18}}\right)^{-(\gamma-1)/2} \tag{13}$$

(Lang 1980, Sect. 1.26), where ν and γ are the frequency and the spectral index, respectively, of the electron energy distribution and $c(\gamma)$ is a known slowly varying function of γ, e.g. $c(2.8) = 1.65$ and $c(2.4) = 1.79$. In Eq. (13) only the mean magnetic field is included, because we do not have adequate knowledge of the additional, turbulent, field component. We determine the constant K by assuming energy equipartition between the magnetic field and the cosmic rays. This yields, in gaussian cgs units

$$K = 0.01(\gamma - 2) E_{\rm min}^{\gamma-2} \boldsymbol{B}^2/8\pi, \tag{14}$$

with $E_{\rm min} = 300$ MeV, $\gamma = 2.8$ (Beck 1991), and gives

$$\varepsilon\, ds = 5\,10^4 \frac{\rm Jy}{\rm sr} \left(\frac{|\boldsymbol{B}_\perp|}{5\mu{\rm G}}\right)^{1.9} \left(\frac{|\boldsymbol{B}|}{5\mu{\rm G}}\right)^{2} \left(\frac{\nu}{1.5{\rm GHz}}\right)^{-0.9} \left(\frac{ds}{15{\rm kpc}}\right). \tag{15}$$

($\nu = 1.5$ GHz corresponds to 20 cm wavelength.)

We also give some synthetic maps including internal Faraday depolarisation, i.e. we integrate the Stokes Q and U parameters

$$Q = -\int_{-\infty}^{\infty} p_0 \varepsilon \cos(2\chi + F) ds, \tag{16}$$

$$U = -\int_{-\infty}^{\infty} p_0 \varepsilon \sin(2\chi + F) ds, \tag{17}$$

where p_0 is the degree of polarisation of the emitted radiation, χ is the orientation angle of the electric field vector (perpendicular to the magnetic field), $F = F(s)$ is the Faraday depth

$$F(s) = \int_{s}^{\infty} f(s') ds', \tag{18}$$

(the observer is located at $s = +\infty$), and f is the differential Faraday rotation rate with

$$f ds = 4800 \left(\frac{n_{\rm th}}{1{\rm cm}^{-3}}\right) \left(\frac{B_\parallel}{5\mu{\rm G}}\right) \left(\frac{\nu}{1.5{\rm GHz}}\right)^{-2} \left(\frac{ds}{15{\rm kpc}}\right) \tag{19}$$

(see e.g. Cioffi & Jones 1980). For the distribution of thermal electrons we assume a simple profile

$$n_{\rm th} = \sum_{i=1}^{3} n_e^{(i)} \exp(-\varpi/\varpi_{\rm th}^{(i)}) \exp(-|z|/z_{\rm th}^{(i)}). \tag{20}$$

The distribution of thermal electrons in NGC 891 has been studied by Rand et al. (1990) and Dettmar (1990). Although their models differ somewhat, they find a component with a scale height of about one kpc, a radial scale length of a few kpc, and electron densities in the centre of about $n_e \approx 0.1...0.5\,{\rm cm}^{-3}$. We use the values given by Sukumar & Allen (1991): $\varpi_{\rm th}^{(1,2,3)} =$ 2.5, 6.5, 9.0 kpc, $z_{\rm th}^{(1,2,3)} = 1.0$, 0.6, 2.0 kpc and $n_e^{(1,2,3)} = 0.15$, 0.10, $0.03\,{\rm cm}^{-3}$, for the bulge, disc, and halo components, respectively. The Faraday rotation measure produced in the halo is relatively low (of the order of $10\,{\rm rad\,m}^{-2}$) and the Faraday rotation at a wavelengths about 10 cm is negligible outside the disc. Thus, for the polarisation maps presented in this paper we either considered a wavelength short enough that Faraday rotation may be neglected, or we took a wavelength of 20 cm.

For a field of strength a few μG, the emission from the disc is depolarised by the differential Faraday rotation from Eq. (19) alone. In addition there is a contribution to depolarisation from the small scale magnetic fields, but we neglect this effect here.

3.1. Polarisation maps

Below we present the results in terms of maps of the polarised intensity $PI \equiv (Q^2 + U^2)^{1/2}$ and unsigned magnetic field vectors, determined from the synthetic polarisation vectors for an observer viewing the galaxy edge-on. Details of the method and several examples may be found in Donner & Brandenburg (1990b). Similar synthetic polarisation maps have also been studied by Elstner et al. (1992). In Sect. 5 we give pictures of the geometry of the poloidal magnetic field together with the corresponding maps showing the distribution of polarised emission and intensity for a number of the models. For the sake of clarity we have mostly considered short wavelength and have then neglected the Faraday rotation (i.e. the F-term in Eqs. (16) and (17)). For larger wavelength this effect would cause an asymmetric appearance of the polarisation maps and an almost random orientation of the field vectors in the inner parts. In the halo these distortions are not very strong because of a low Faraday rotation measure there. In Sect. 5.6 and Fig. 13 we show some examples of this, where we have restored the F-term in the computation of the Stokes parameters.

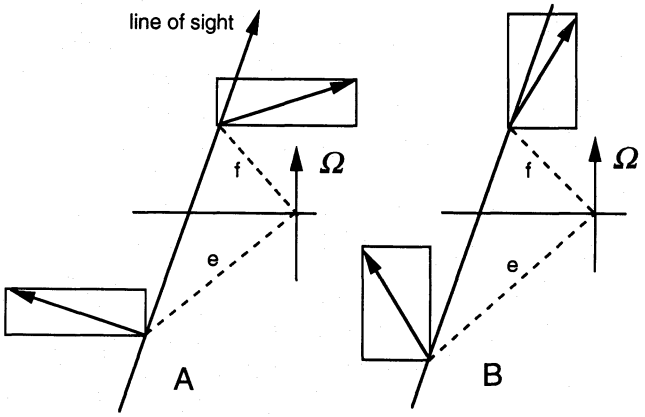

Fig. 5. Sketch illustrating the cancellation effect for the polarisation from B-vectors with $B_\varpi = 0$ that are located an equal distance from the rotation axis ($e = f$). In the two cases the Stokes U parameter cancels to zero, whilst the resulting polarisation vector χ_E is zero for the case A and 90° for case B

It should be remembered that the emission at any point is never fully polarised ($p_0 \le 3(\gamma+1)/(3\gamma+7)$). Thus, the electric field has components not only in the direction of polarisation, but also perpendicular to it. By superimposing electric field vectors with different polarisation angles, the components in the direction of polarisation and perpendicular to it become more and more equal. Thus, the polarised intensity PI decreases. Unless $PI \equiv 0$ we can always determine the resulting polarisation angle χ_E, but for small values of PI the significance of χ_E decreases and the noise level increases.

3.2. A geometrical effect in synthetic polarisation maps

It is apparent in some of the polarisation maps presented below that polarisation vectors can be purely horizontal in large volumes far above the galactic plane. This is not necessarily due to the dominance of the toroidal field but rather to a cancellation effect occurring for an axisymmetric field geometry with $B_\varpi \equiv 0$, and negligible Faraday rotation. In order to illustrate this situation we have drawn in Fig. 5 pairs of magnetic field vectors along the line of sight that are located an equal distance from the rotation axis ($e = f$ in Fig. 5). Because of axisymmetry and $B_\varpi \equiv 0$, the two vectors only differ in the sign of the horizontal component. Thus, the corresponding orientation angles of the electric field, χ^+ and χ^-, satisfy $\chi^+ = \pi - \chi^-$. This gives contributions to the Stokes Q and U parameters

$$Q \sim -\cos 2\chi^+ - \cos 2\chi^- = -2\cos 2\chi^+, \tag{21}$$

$$U \sim -\sin 2\chi^+ - \sin 2\chi^- = 0. \tag{22}$$

The polarisation angle of the electric field vector is given by $\chi_E = \frac{1}{2}\arctan(U/Q)$, and the angle of the magnetic field vector

by $\chi_B = \chi_E + \pi/2$. Since $U \equiv 0$, but Q is either positive or negative, we have

$$\chi_E = \begin{cases} \pi/2 & \text{for } |\chi^+| > \pi/4 \ (caseA), \\ 0 & \text{for } |\chi^+| < \pi/4 \ (caseB). \end{cases} \quad (23)$$

Thus, the polarisation vectors of the electric field are either vertical or horizontal, and the synthesised magnetic field vectors either horizontal (case A) or vertical (case B).

Of course, a nonzero radial field component destroys the exact cancellation. Also deviations from exactly axisymmetric field and cosmic ray electron distributions produce a nonvanishing Stokes U component. Thus the cancellation effect is unlikely to be significant in real galaxies, but it strongly affects our synthetic polarisation maps if Faraday rotation is weak or the wavelength short. We should bear this in mind when comparing our maps with observations.

4. Idealised models

In order to clarify physical effects associated with individual ingredients of our models, we briefly summarise in this section some results obtained at an early stage of this work, using idealised models without diamagnetism that ignore the dependence of α on Ω and with isotropic α effect and thicker discs, similar to the models presented in Paper I.

Models with small values of C_Ω (around one hundred) have the property that the resulting field vectors in the polarisation maps are almost radially oriented above the disc plane. However, as we increase C_Ω to more realistic values around 600 the synthetic field vectors become almost horizontal, because the halo toroidal field begins then to dominate over the poloidal one.

The contours of polarised intensity are normally elliptically shaped. The maximum emission comes from the centre even though the field there is quite weak. This is, however, only a projection effect, since here the line of sight through the galaxy is the longest. In the presence of a weak galactic wind the poloidal field becomes more nearly radial in the outer parts, $r \gtrsim 0.3$. The polarised intensity contours are no longer elliptically shaped, but there are maxima around $r = 0.4$ along the galactic plane. This is in contrast to the intensity distributions observed for NGC 891, but a similar feature is seen in the observed map of NGC 4631 (see Fig. 9 in Hummel et al. 1991b).

In Paper I we found a régime in which an A0 field (antisymmetric about the equatorial plane) in the halo could dominate the disc field. In the absence of a galactic wind such a field is oscillatory and there are significant toroidal fields in the halo, giving horizontal field vectors in the polarisation maps. However, a rather weak galactic wind is sufficient to cause the field to be nonoscillatory. This has dramatic effects on the synthesised magnetic field vectors, which now appear to be vertical close to the galactic disc and radial in the outer parts. However, the field configuration loses these "desirable" features when more realistic parameter values are considered; moreover, the A0 mode is in our models typically less preferred than the S0 mode.

For sufficiently large values of C_Ω and larger values of the disc thickness the S0 solution begins to oscillate. The period is typically about 0.1 diffusion times. The magnetic field belts change over the cycle and migrate towards the equatorial plane where they disappear. The intensity contours typically show maxima above and below the galactic disc, which is quite different from the intensity pattern observed in various edge-on galaxies. It remains an interesting and open question whether or not dynamos producing oscillatory magnetic fields can be satisfactory models for these galaxies.

The presence of a weak galactic wind is in many cases sufficient to change an oscillatory solution into a steady one, but the synthetic magnetic field vectors only become radial far away from the disc. Dynamo action persists for models with thick discs even for quite large wind speeds. In this case the field in the halo is extremely weak, and the synthetic magnetic field vectors are strictly radial immediately above and below the disc. The intensity drops abruptly outside the disc. This is not typical of observed intensity distributions, which seem to decrease much more smoothly. Thus, thick-disc dynamos with extremely large wind velocities can perhaps be ruled out in several observed galaxies.

5. More realistic models

In this section we shall focus the discussion on models with the basic parameters relevant to the two galaxies NGC 4631 ($C_\Omega = 1400$, $\varpi_\Omega = 0.1$) and NGC 891 ($C_\Omega = 1040$, $\varpi_\Omega = 0.2$). The adopted values of the other parameters are: $\xi = 0.02$, $h = 0.1$, $z_w = z_W = 0.2$, $z_\Omega = 0.3$, $\eta_1 = 0.95$, unless stated otherwise. The parameters that we varied are $W_r = 0...500$, $W_z = 0...40$, and $\alpha_z = -2... + 4$. In the tables below we give the values of the (nondimensional) magnetic energy, $E_M = \int \frac{1}{2}\boldsymbol{B}^2 dV$, the energy of the poloidal field, E_p, relative to the total energy, $Q = E_p/E_M$, the maximum field strength, $B_{\max}$ and, for oscillatory solutions, the period of the magnetic cycle.

In this section we discuss a number of effects, but we consider those of a radial wind (Sect. 5.2) and turbulent diamagnetism (Sect. 5.4) to be the most important. We note that in previous work on galactic dynamos the rôle of turbulent diamagnetism was not appreciated; we find that, for example, it may force otherwise stationary solutions to be oscillatory. In Figs. 6–15 below we show total intensity contours with synthesised magnetic field vectors superimposed. As long as we neglect the effects of chaotic (small scale) magnetic fields and Faraday rotation is negligible outside the disc polarised intensity contours above the disc are rather close to the total intensity contours shown in our maps.

5.1. Anisotropic α

We begin by investigating the effect of an anisotropic α effect on the magnetic field geometry. Here we use $\varpi_\Omega = 0.1$, a value characteristic of NGC 4631 but, in order to illustrate the effect of an anisotropic α more clearly, we first show the results for $C_\Omega = 700$ instead of 1400; see Fig. 6. We see that there is a trend for a vertical field component to be built up at some distance above the disc plane. At the same time the magnetic energy

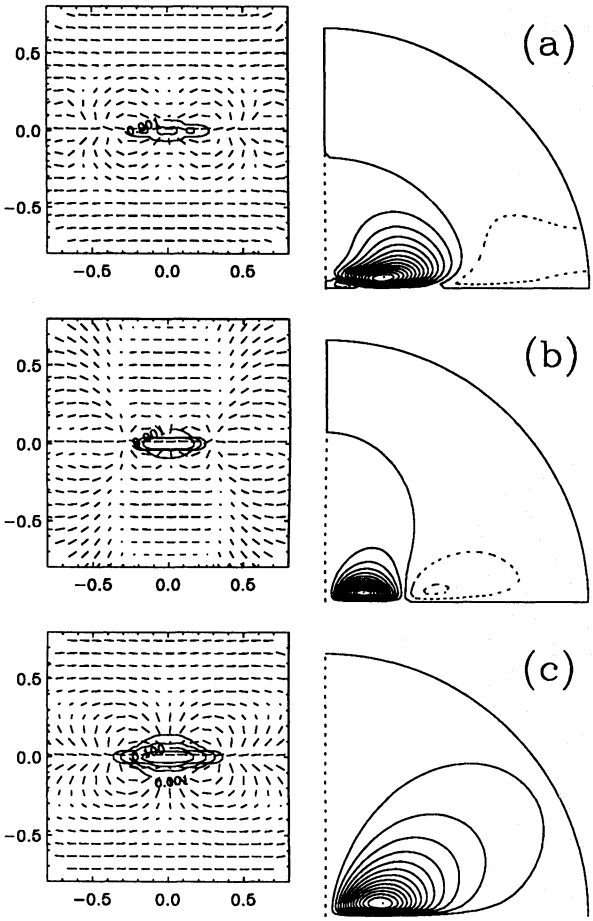

Fig. 6. Polarisation map and poloidal field geometry for a model with $C_\Omega = 700$, $\varpi_\Omega = 0.1$ (a) $\alpha_z = -2$, (b) $\alpha_z = 0$, (c) $\alpha_z = 4$. On the left is shown the orientation of the magnetic field determined from the Stokes parameters, where the angle is $\arctan(U/Q) + \pi/2$ and the length of the vectors is proportional to the degree of polarisation, PI/I. Logarithmically spaced contours (interval is a factor of 10) of the total intensity are superimposed. On the right are shown field lines of the poloidal field in one quadrant of a meridional plane. The outer halo boundary at $r = R$ is marked

Table 1. The effect of the anisotropic α-effect on the results for a model with $C_\Omega = 700$, $\varpi_\Omega = 0.1$, $W_r = W_z = 0$

α_z	ξ	$\lg E_M$	Q	$B_{\max}$	$T_{\rm cyc}$
−2	0.05	−2.66... − 2.31	0.40...0.57	0.7...1.0	0.06
0	0.03	−2.14	0.32	1.9	
2	0.03	−1.93	0.23	2.0	
4	0.02	−1.54	0.18	2.6	

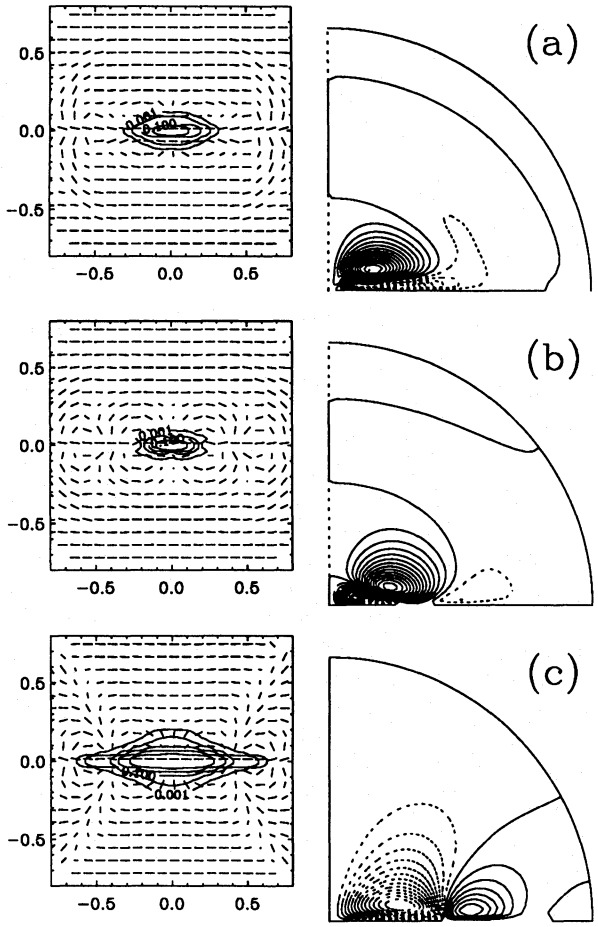

Fig. 7. Polarisation map and poloidal field geometry at an arbitrarily chosen phase for a model using the rotation curve parameters of NGC 4631 and different strengths of anisotropy, for $C_\Omega = 1400$, $\varpi_\Omega = 0.1$, $\xi = 0.02$, $W_r = W_z = 0$. (a) $\alpha_z = -2$, (b) $\alpha_z = 0$, (c) $\alpha_z = 2$

increases, which shows that the α_z term contributes to dynamo action; see Table 1. In the cases $\alpha_z = 0$ and 2 we have used $\xi = 0.03$, instead of $\xi = 0.02$, because the value of C_Ω is so small that otherwise the α effect is not large enough to support dynamo action.

Note that the solutions for $\alpha_z \geq 0$ are steady. In this context is should be recalled that anisotropies in α sometimes lead to oscillatory behaviour in spherical dynamos (Weisshaar 1982). In fact, the solution for $\alpha_z < 0$ is oscillatory, but the dynamo is so weak that we had to choose $\xi = 0.05$ in order to obtain dynamo action (see Table 1).

The behaviour for $C_\Omega = 1400$ is different in that the solution is oscillatory already in the absence of the α_z term (see Table 2). The resulting field geometry is shown in Fig. 7. It is notable that the radial profile of the field near to and within the disc has pronounced reversals. As the degree of anisotropy increases the solution becomes steady and stronger horizontal fields develop. Our current results do not provide strong evidence that the global vertical structure of the field high in the halo might be caused by anisotropies in α.

5.2. *The effect of a radial wind*

In Table 3 and Fig. 8 we show the results for a model with the rotation curve parameters of NGC 4631 ($C_\Omega = 1400$, $\varpi_\Omega = 0.1$), for different strengths of the radial component of the wind and $\alpha_z = 0$. We have seen in Table 2 that in the absence of a wind the

Table 2. The effect of the anisotropic α-effect on the results for a model using the rotation curve parameters of NGC 4631. For oscillatory solutions the minimum and maximum values of lg E_M, Q, and $B_{\rm max}$ are given. $C_\Omega = 1400$, $\varpi_\Omega = 0.1$, $\xi = 0.02$, $W_r = W_z = 0$

α_z	lg E_M	Q	$B_{\rm max}$	$T_{\rm cyc}$
−2	−3.4... − 2.8	0.25...0.45	0.4...0.9	0.04
−1	−2.53... − 1.94	0.18...0.44	0.7...2.4	0.10
0	−2.00... − 1.47	0.13...0.26	2.7...4.5	0.15
2	−0.81	0.10	6.6	
4	−0.51	0.08	7.7	

solution is oscillatory. In Sect. 5.4 we show that this property is a consequence of the turbulent diamagnetic effect included here. When the wind strength in the radial direction increases the solution becomes steady and both the magnetic energy and the maximum magnetic field strength increase with increasing values of W_r up to 200. This is partly due to the fact that a not too large wind velocity tends to counteract the effect of diamagnetism in decreasing the magnetic energy, presumably because of the compression of the field into a thinner disc without enhancing the field strength; see Sect. 5.4. This is an unexpected and important result: for moderate wind velocities the wind facilitates the galactic dynamo rather than inhibits it.

A remarkable consequence for larger wind velocities (around 500) is that the solutions again become oscillatory; see Table 3. A possible reason for this might be that the field is then so effectively pushed into the outer parts of the disc so that the field geometry becomes similar to the case of a dynamo in a sphere. Because of this surprising behaviour we have checked the numerical accuracy of this solution for higher resolution (63×64) and found quantitatively similar results.

Note that the synthetic magnetic field vectors become more nearly radially oriented as the wind speed increases. For $W_r = 200...500$ the resulting field vectors align with the velocity vectors and it is conceivable that the field geometry observed in NGC 4631 might be reproduced by a suitably chosen wind profile.

We should stress that the effect of the wind on the dynamo cannot be reduced to a simple advection. Since the wind flow is axisymmetric, such advection by itself could only lead to the enhancement in the halo of the toroidal field that dominates in the disc. The wind rather leads to more subtle changes in the dynamo associated with stretching of magnetic field lines by velocity shear.

In Table 4 and Fig. 9 we show the results for a model using the rotation curve parameters of NGC 891 ($C_\Omega = 1040$, $\varpi_\Omega = 0.2$) for different strengths of the radial wind. Note that even for rather large wind velocities the synthetic field vectors are more nearly parallel to the disc plane and not much affected by the wind. This is consistent with the observations of NGC 891 and NGC 4565.

In order to clarify the question why the effect of the wind is so weak in the case where we use the rotation curve of NGC 891, we now consider an intermediate case between this model and the model for NGC 4631, using $\varpi_\Omega = 0.15$ and $C_\Omega = 1400$

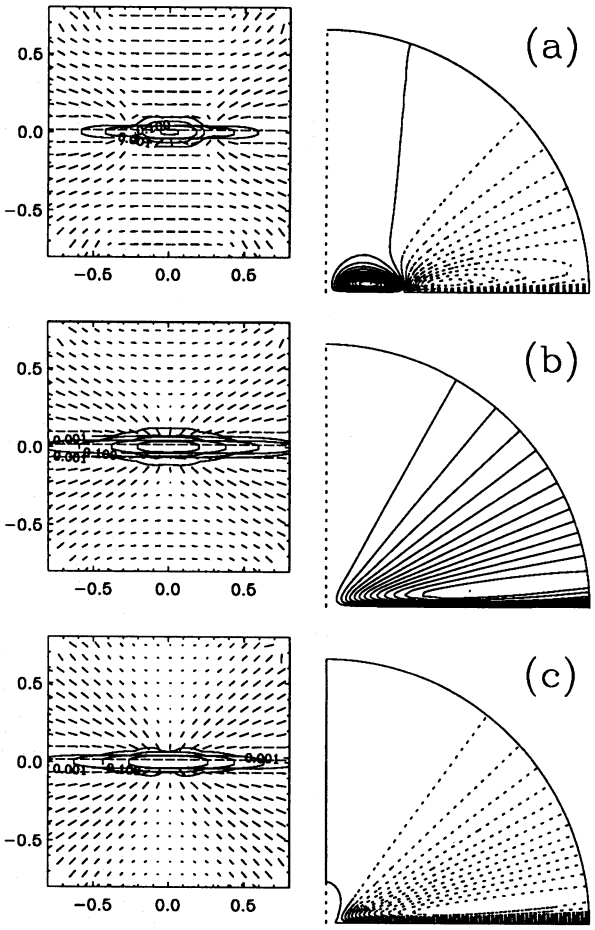

Fig. 8. Polarisation map and poloidal field geometry for a model using the rotation curve parameters of NGC 4631 and different wind strengths: (a) $W_r = 50$, (b) $W_r = 200$, (c) $W_r = 500$. The case with $W_r = 0$ is depicted in panel (a) of Fig. 3. Here, as well as in the other polarisation maps, vectors are only shown where PI exceeds 2% of the maximum value. $C_\Omega = 1400$, $\varpi_\Omega = 0.1$, $\xi = 0.02$, $\alpha_z = 0$, $W_z = 0$

Table 3. Results for a model using the rotation curve parameters of NGC 4631 and different values of W_r. $C_\Omega = 1400$, $\varpi_\Omega = 0.1$, $\xi = 0.02$, $\alpha_z = 0$, $W_z = 0$

W_r	lg E_M	Q	$B_{\rm max}$	$T_{\rm cyc}$
0	−2.00... − 1.47	0.13...0.26	2.7...4.5	0.15
50	−1.42	0.15	4.0	
200	−0.78	0.14	4.7	
500	−1.19... − 1.19	0.19...0.30	1.5...3.4	0.14

Table 4. Results for a model using the rotation curve parameters of NGC 891 and different values of W_r. $C_\Omega = 1040$, $\varpi_\Omega = 0.2$, $\xi = 0.02$, $\alpha_z = 0$, $W_z = 0$

W_r	lg E_M	Q	$B_{\rm max}$	$T_{\rm cyc}$
0	−1.00... − 0.89	0.15...0.18	3.2...4.4	0.10
50	−1.12... − 1.04	0.18...0.21	2.2...3.4	0.07
200	−1.69... − 1.53	0.25...0.28	1.5...2.2	0.06

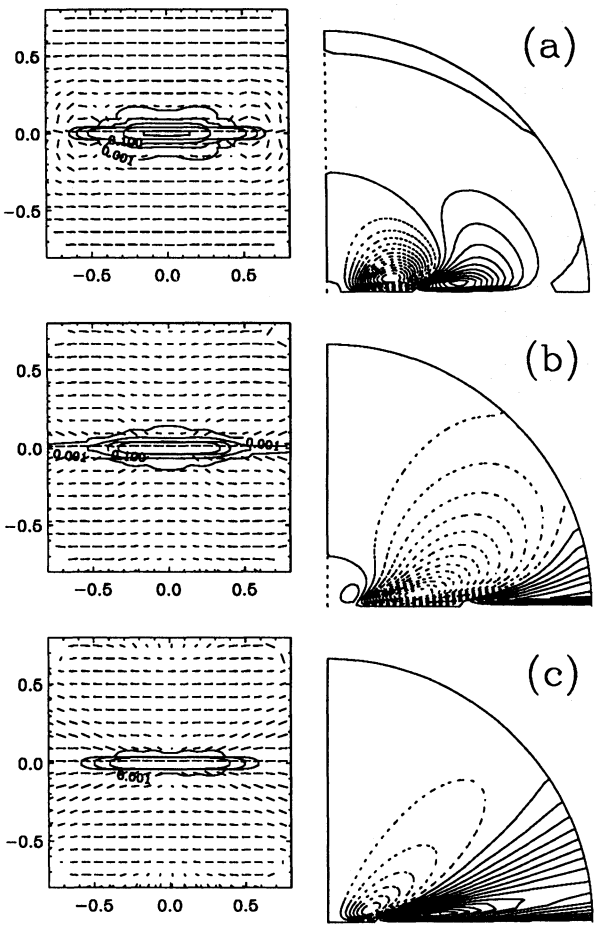

Fig. 9. Polarisation map and poloidal field geometry for a model using the rotation curve parameters of NGC 891 and different wind strengths, for $C_\Omega = 1040$, $\varpi_\Omega = 0.2$, $\xi = 0.02$, $\alpha_z = 0$, $W_z = 0$. (a) $W_r = 0$, (b) $W_r = 50$, (c) $W_r = 200$

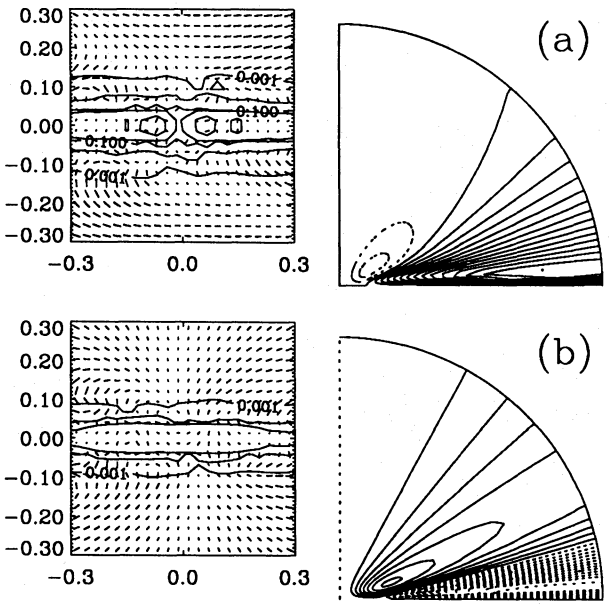

Fig. 10. Polarisation map and poloidal field geometry for an intermediate model between NGC 891 and NGC 4631 and different wind strengths, for parameters $C_\Omega = 1400$, $\varpi_\Omega = 0.15$, $\xi = 0.02$, $\alpha_z = 0$, $W_z = 0$, and Faraday rotation is included. Only the inner region with $\varpi, z \leq 0.3$ is shown. (a) $W_r = 200$, (b) $W_r = 500$

for two different values of the radial wind strength. According to more recent observations this may actually be the value appropriate for NGC 4631; see Sect. 2.2. The result is shown in Fig. 10. In this figure we have only focussed on the innermost parts, because this is the region studied in many observational polarisation maps. Here we have also included the effects of Faraday rotation; see Sect. 5.6. From the resulting field geometry, shown in Fig. 10, it seems that this case is intermediate between those displayed in Figs. 8 and 9. Thus, the field geometry is rather sensitive to ϖ_Ω, but less sensitive to small changes in the value of C_Ω. Because of the effects of Faraday rotation there are regions with rather different field orientations, similar to those shown by the vectors in Fig. 1.

5.3. The effect of a vertical wind

In Table 5 and Fig. 11 we show the results for a model using the rotation curve parameters of NGC 4631 ($C_\Omega = 1400$, $\varpi_\Omega = 0.1$) for different strengths of the wind in the vertical direction, W_z. The presence of a vertical wind close to the disc plane seems to enhance dynamo action, because it pushes field from the galactic plane into the regions above and below where the extrema of α are located. However, only E_M increases significantly with W_z, whereas $B_{\max}$ remains unchanged, because it is limited by α-quenching at a level independent of the wind strength.

The vertical wind transports a strong toroidal field from the disc into the halo thereby making the magnetic vectors more nearly horizontal. The result presented in Fig. 11 seems to imply that W_z in NGC 4631 is unlikely to exceed approximately 20 km/s. Remember that this value of W_z applies to the location $z = z_W = 0.2\,R$ which is much closer to the disc than the distance $r = R$ to which the values of W_r refer. The critical value of W_z is close to our simple estimate Eq. (1). Note that with S0 geometry the field near the galactic planes is approximately perpendicular to the vertical wind, which favours this naive estimate.

Table 5. Results for a model using the rotation curve parameters of NGC 4631 and different values of W_z. Note that $B_{\max}$ is independent of W_z, but that E_M increases with W_z. $C_\Omega = 1400$, $\varpi_\Omega = 0.1$, $\xi = 0.02$, $\alpha_z = 4$, $W_r = 200$

W_z	$\lg E_M$	Q	$B_{\max}$
0	−0.51	0.12	5.9
20	−0.27	0.04	5.9
40	+0.09	0.01	5.9

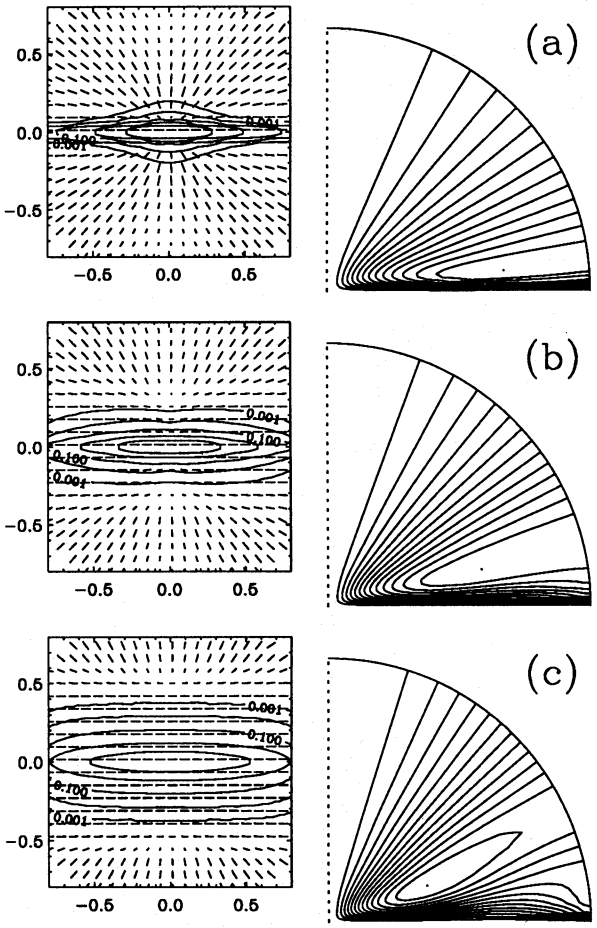

Fig. 11. Polarisation map and poloidal field geometry for a model using the rotation curve parameters of NGC 4631 with a radial wind and different vertical wind strengths, for $C_\Omega = 1400$, $\varpi_\Omega = 0.1$, $\xi = 0.02$, $\alpha_z = 4$, $W_r = 200$. (a) $W_z = 0$, (b) $W_z = 20$, (c) $W_z = 40$

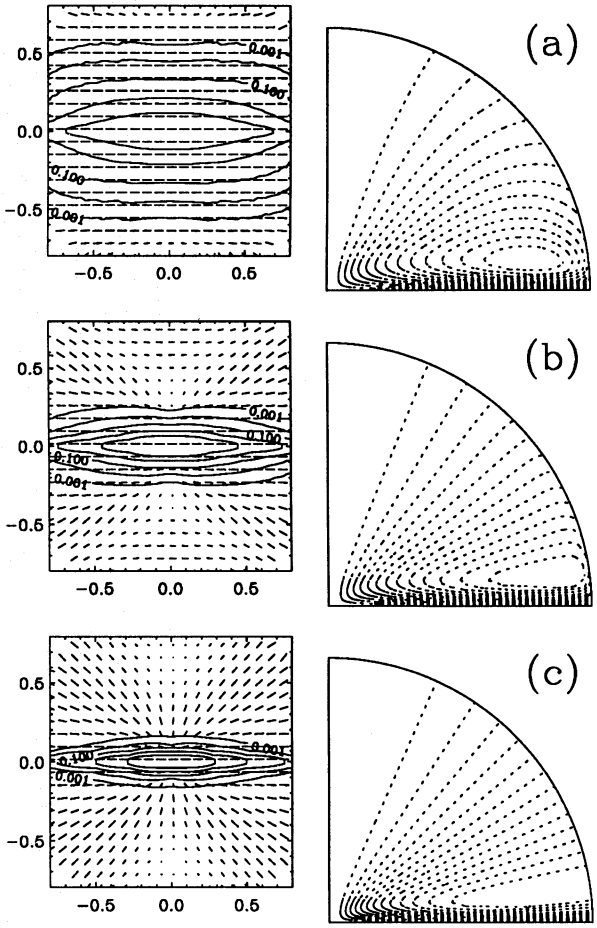

Fig. 12. Polarisation map and poloidal field geometry for models with turbulent diamagnetism omitted. The rotation curve parameters are those of NGC 4631, for $C_\Omega = 1400$, $\varpi_\Omega = 0.1$, $\xi = 0.02$, $\alpha_z = 0$, $W_z = 0$. The radial wind strengths are (a) $W_r = 0$, (b) $W_r = 50$, (c) $W_r = 200$

5.4. Turbulent diamagnetism

We recall that in the absence of a galactic wind the solutions obtained are oscillatory. This is surprising, because it is known that for thin discs the solutions of S0 parity are normally steady. In order to isolate the mechanism responsible for this we have considered models where the turbulent diamagnetic effect is suppressed, by putting $\gamma = 0$. The results are shown in Table 6 and Fig. 12, and should be compared with the cases with diamagnetism included; see Table 3 and Figs. 7b and 8a,b. In the absence of turbulent diamagnetism we indeed obtain steady solutions, as expected. Thus, in the context of galaxies, turbulent diamagnetism can cause the solutions to become oscillatory. For spherical dynamos the turbulent diamagnetism often causes oscillatory solutions to become steady (e.g. Rädler 1986). The resulting magnetic field strength is larger when the turbulent diamagnetic effect is suppressed. This is consistent with the fact that a weak wind can support the dynamo because it may counteract the turbulent diamagnetism.

We should emphasise that the turbulent diamagnetism of galaxies behaves in a somewhat unusual way, in that it pushes magnetic field into the disc so that the scale height of the magnetic field is considerably smaller than that of the gas (cf. Poezd et al. 1992). (In stellar convection zones, for example, turbulent diamagnetism transports magnetic field away from the bulk of convection zones, i.e. to the surface and to the bottom of the convection zone.) Note in this connection that the rotation measure analysis of extragalactic radio sources and pulsars yields a scale height of the magnetic field in the disc of 400...500 pc in the Milky Way (Ruzmaikin et al. 1988, Sect. 4.3), whilst the scale height of the Reynolds disc is approximately 1.5 kpc (see Reynolds 1989). Local enhancements of the poloidal field and corresponding reversals in the toroidal field which can be seen in Fig. 7b are also associated with the effects of turbulent diamagnetism. In NGC 4631 the situation is rather different, in that there the presence of a wind counteracts the diamagnetic effect, and the scale height of the magnetic field is much greater than that of the gas (Hummel et al. 1991b).

Table 6. Results for models without the turbulent diamagnetic effect using the rotation curve parameters of NGC 4631 and different values of W_r. $C_\Omega = 1400$, $\varpi_\Omega = 0.1$, $\xi = 0.02$, $\alpha_z = 0$, $W_z = 0$

W_r	$\lg E_M$	Q	$B_{\max}$
0	+0.46	0.01	8.0
50	−0.02	0.04	6.9
200	−0.46	0.07	5.4

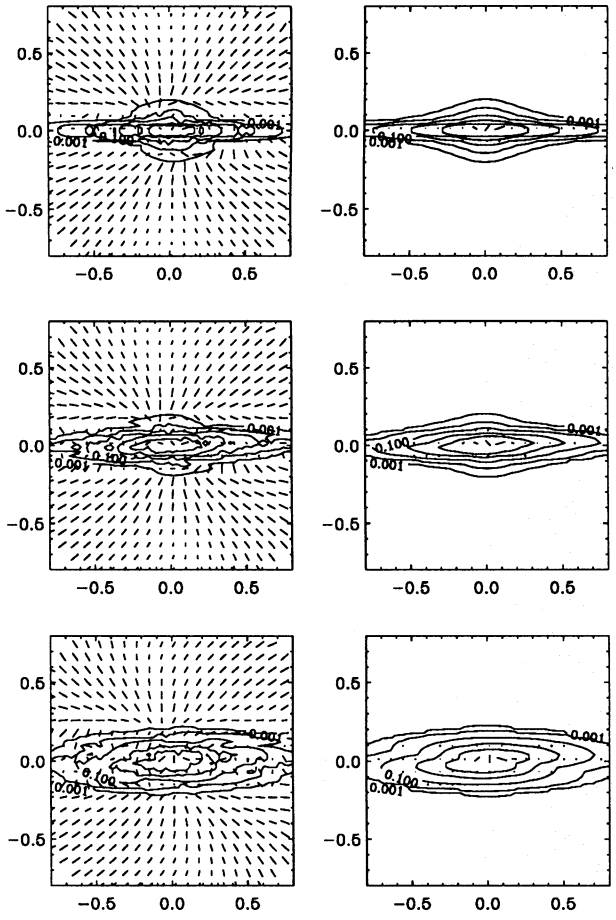

Fig. 13. Polarisation maps for a model with $C_\Omega = 1400$, $\varpi_\Omega = 0.1$, $\xi = 0.02$, $\alpha_z = 4$, $W_r = 200$, $W_z = 0$ and with Faraday rotation included. On the left hand side we show contours of PI and polarisation vectors with a length proportional to PI/I, and on the right hand side contours of I and polarisation vectors with a length proportional to PI. The inclination angle is, from top to bottom respectively, 90°, 85° and 80°

5.5. Vertical dependence of Ω

We made some comparisons between models with and without a z-dependence of Ω by considering various values of z_Ω. It turned out that the solutions are not very sensitive to this change and, in particular, that the oscillatory solutions for $C_\Omega = 1400$, $\varpi_\Omega = 0.1$, $W_r = 0$, and $\alpha_z = 0$ remain oscillatory, independently of the presence or absence of an Ω gradient in the z direction. The magnetic energies of the solutions remain quite similar, but the polarisation maps for the solutions with Ω constant on cylinders

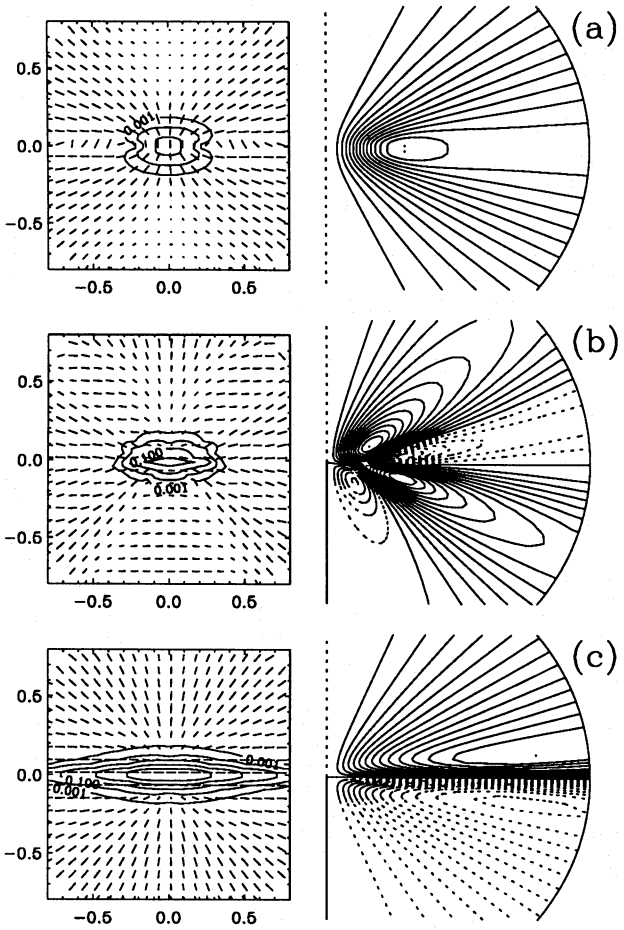

Fig. 14. Polarisation map and poloidal field geometry for solutions with pure dipole (a), mixed (b), and pure quadrupole (c) symmetry. The rotation curve parameters are those of NGC 4631. (For technical reasons the location of the vectors is not chosen symmetrically about the disc plane.) $C_\Omega = 1400$, $\varpi_\Omega = 0.1$, $\xi = 0.02$, $\alpha_z = 4$, $W_r = 200$, $W_z = 0$

(i.e. for $z_\Omega \to \infty$) tend to show vertical features that are absent in the case of a z-dependent Ω, and which seem to be absent in observed field configurations.

5.6. Intrinsic Faraday rotation and depolarisation

Both the effects of Faraday rotation and of an inclination angle differing from 90° can cause asymmetries in the resulting polarisation maps. Examples of polarisation maps for different inclination angles are shown in Fig. 13, where we have included the Faraday rotation in the computation of the Stokes parameters. Note that there is now a strong depolarisation in the disc resulting in shorter polarisation vectors (length PI/I), with a somewhat irregular appearance. The field vectors in the halo are not strongly affected by the inclusion of Faraday rotation because the low number density of thermal electrons gives only weak Faraday rotation there. It is notable that the polarisation pattern high in the halo, unlike that closer to the disc, is rel-

atively stable with respect to Faraday rotation and inclination effects.

At inclination angles around 80° the I-contours show asymmetry about the disc plane. Similar behaviour is observed in NGC 253, where the inclination angle is 78° (Klein et al. 1983).

5.7. Stability and mixed parity

For some cases we checked the stability of the solutions obtained to axisymmetric perturbations. We typically find that the S0 solutions presented in this paper are stable. However, A0 solutions were also found to be stable in most of the cases, but only under weak perturbations. (It is possible that these weakly stable A0 solutions are unstable with respect to nonaxisymmetric perturbations, by analogy to similar results for dynamos in a sphere; see Rädler & Wiedemann 1989, Jennings et al. 1990). Since the magnetic diffusion time scale for galaxies is typically rather long, it is relevant also to consider transient solutions (see Paper I). In Fig. 14 we compare the field geometries of the A0 and S0 solutions with that of such a transient solution with mixed parity. The energies of the A0 and mixed parity solutions are smaller than the energy of the S0 solution. We stress that all three basic types of dynamo solutions are potentially relevant for the observed polarisation patterns: galaxies are not necessarily old enough for the final stable state to have been reached (e.g. Paper I). We postpone a detailed analysis of these possibilities to our future papers.

5.8. Larger correlation length

The parameters of interstellar turbulence in the Reynolds disc and galactic halo are rather uncertain, so that it is worthwhile investigating other possibilities than those considered above. In particular, the scale length of turbulent motions ℓ might be comparable to the scale height of the thick disc provided that the turbulence above the height of 500 pc is driven by superbubbles, Parker instabilities, etc., which suggest a typical scale of 1...1.5 kpc. Larger values of ℓ result in a larger ratio C_α/C_Ω, i.e. a smaller relative rôle of differential rotation in the dynamo, thereby leading to relatively larger poloidal magnetic field. We also take $u_t = 40$ km/s in this model, which might be more suitable for such a thick disc.

Thus, we also considered a model with $\ell = \mathcal{O}(0.1)$, $u_t = 40$ km/s and $\gamma = 0$. For such large ℓ and smaller u_t it is important to note that $|\alpha| \sim \min(\ell^2\Omega/h, u_t)$. In Fig. 15 we present polarisation maps for a model with isotropic α-effect, no wind, and $C_\Omega = 700$, $\varpi = 0.1$.

We note that in the model with large ℓ the field has a reversal near the disc plane, with corresponding symmetric enhancements of polarised intensity at the distance of a few kpc from the rotation axis. The field structure is rather complicated but near the reversals there is a tendency for the magnetic vectors to be vertically oriented.

Summarising the experience gained from the models with larger ℓ and anisotropic α, we can say that these two effects can both lead to local dominance of the vertical field within regions

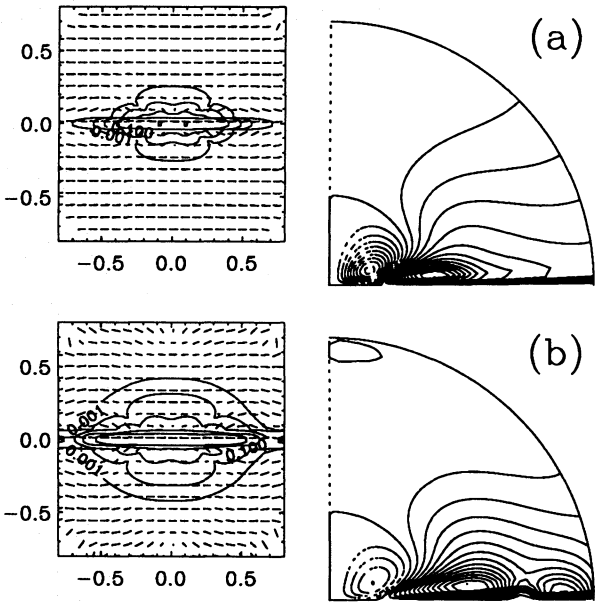

Fig. 15. Polarisation map and poloidal field geometry for solutions with $C_\Omega = 700$, $\varpi_\Omega = 0.1$, $\xi = 0.02$, $\alpha_z = W_r = W_z = 0$. Only the inner region with $\varpi, z \leq 0.3$ is shown. $\xi = 0.05$ (a) and $\xi = 0.10$ (b)

of 1...1.5 kpc in size, with the anisotropy yielding more pronounced vertical fields (see Fig. 6). However, a global pattern with the vertical magnetic field dominating, appears to be associated with the effects of a radial galactic wind. Note also that models with such a wind can also feature field reversals near to and within the disc, even for isotropic α and a conservative value of ℓ (Fig. 7a and 8).

6. Discussion

The main results of this paper are as follows: In our model we have considered the interaction of the wind with the dynamo in a relatively thick disc with a scale height of about 1.5 kpc surrounded by a spherical halo. We expect that in a galaxy such as NGC 4631 the regular magnetic field is generated mainly within the disc and carried away to the halo by the wind. The global dominance of the poloidal magnetic field above the disc of NGC 4631 can be explained by the effect of the (nearly) radial wind on the galactic dynamo. We consider the model presented in Figs. 8b and c, where the radial wind is included, or that of Fig. 13 (where, in addition, an anisotropy of α is included), to be the most relevant for NGC 4631 (cf. Fig. 1). If our models of the magnetic field in the galactic halo are correct we expect the radial wind speed of NGC 4631 to be around 200 km/s at the edge of the halo.

When the dynamo is also active in the galactic halo or there is no wind, then the toroidal field dominates both in the disc and in the halo, at least in the framework of the models considered here, which have magnetic field symmetry of S0 type. Thus, the magnetic field configurations observed in such galaxies as NGC 891 and NGC 4565 are compatible with either a relatively strong halo dynamo or a weaker galactic wind. The field config-

urations presented in Fig. 9 would seem to be more appropriate for the latter two galaxies (cf. Fig. 2).

Wind speeds of 50...200 km/s in the outer parts of the halo are generally admissible, in that they can still allow the dynamo to work. This is due to the partial alignment of the magnetic field and the wind, and the anchoring of the field lines in the disc.

Both an anisotropic α effect and the turbulent diamagnetism can make the magnetic field vectors more aligned with the radial or vertical directions. A vertical component of the wind near the galactic disc leads to a dominance of toroidal field in the halo. In this connection it is useful to emphasise that we always refer to the synthesised magnetic field vectors and not to those projected onto meridional planes.

The presence of a vertical wind has quite remarkable effects leading to large magnetic field energies. However, this also causes strong toroidal fields above the disc plane and almost horizontal field vectors in the polarisation maps. Such a configuration could be compatible with observations of NGC 891 and 4565, but not with that observed in NGC 4631, and we therefore expect that in the latter galaxy the vertical wind component close to, or in, the disc should be weak. This inference is consistent with the fact that star formation activity in this galaxy occurs predominantly in the central regions so that the wind can be expected to be nearly radial.

Turbulent diamagnetism has important effects on the properties of the solutions and in particular on the field geometry. In the presence of turbulent diamagnetism and for weak wind velocities the solutions show a reversal of the poloidal field (e.g. Figs. 7 and 9) and also of the toroidal field (not illustrated) at $\varpi = 2...10$ kpc. A similar field reversal is also observed in the Milky Way. Polarisation maps for the field distribution with a reversal show a distinctive shape of the intensity contours, with two local enhancements located symmetrically with respect to the rotation axis at the galactocentric distances of 1...2 kpc, approximately at the positions where the rotation curve becomes flat (see e.g. Figs. 8a, 9, 10). This indicates that the observable poloidal field lying in the plane of the sky is enhanced in the reversal region: magnetic lines bend upwards near the reversal. It is interesting that similar symmetric enhancements of polarised intensity contours are observed in NGC 891 (see Fig. 1b in Sukumar & Allen 1991) and NGC 4631 (see Fig. 5 in Golla & Hummel 1992). We suggest that the symmetric enhancements of the polarised intensity near the disc at the distance of about 2 kpc from the centre of NGC 4631 can be interpreted as being the possible result of a reversal of the large scale magnetic field in the disc of this galaxy. This suggestion can be tested when the maps of Faraday rotation measure become available, because the associated reversing toroidal magnetic field must produce a change in the sign of RM in the same regions.

An interesting peculiarity of the vertical distribution of the degree of polarisation in NGC 891 is its asymmetry with respect to the galactic midplane, indicating a relatively weak regular magnetic field just above the disc on its north-east side (Sukumar & Allen 1991). Such a feature was discussed by Sokoloff & Shukurov (1990) (see also Paper I). It was argued there that the regular magnetic fields in the disc and in the halo can have opposite parities (or, in other words, the global field is of mixed parity), so that on the one side of the disc there will be a magnetic neutral layer whose thickness is about the disc (half-) thickness or 0.5...1 kpc. Note that a small asymmetry is also predicted from internal Faraday depolarisation. As shown in Fig. 13, if the disc is not exactly edge-on, then this will also produce an apparent asymmetry, but this effect is perhaps not large enough to be observationally significant.

It might appear slightly worrying that in all our models the value of ξ is rather large, corresponding to a maximum value of α of about 20 km/s in dimensional units, which is attained at a height of about 1 kpc. This value of α is considerably larger than the value usually adopted for a thin galactic disc (1 km/s). However, α is here evaluated at some height above the disc, and since there the turbulent velocities are larger than in the immediate vicinity of the disc plane, reaching 35 km/s at $z = 1.5$ kpc (Reynolds 1989) and probably 100 km/s in the halo, we expect that this value of α may still be reasonable.

The dimensionless values of the maximal field strength varies in the different models between 0.7 and 8 (see Tables 1-6). This would correspond to dimensional values between approximately 3 and 40 G. These values might appear rather large, but a more representative figure is the average field strength in the inner part of the disc. A crude estimate may be obtained from E_M using $\langle B\rangle_{\rm disc} = (2E_M/V_{\rm disc})^{1/2}$, where $V_{\rm disc} = 2h\pi\varpi^2$). In Table 7 we give a conversion from the $\lg E_M$ values given in Tables 1-6 to dimensional values of the magnetic field strength averaged over this inner part of the disc with a height of 1.5 kpc and a radius of 7.5 kpc ($k = 1$). For intermediate values of W_r our models shown in Tables 3 and 4 have typical values of $\lg E_M$ around -1. This corresponds then to $\langle B\rangle_{\rm disc} = 5.6\mu$G. We should keep in mind that the quenching expression Eq. (8) is quite empirical. With other quenching formulae the maximum field strengths might be somewhat smaller than the $B_{\rm max}$ values given here. Even accepting Eq. (8), the value of k in Eq. (9) is uncertain.

Table 7. Conversion of $\lg E_M$ values to dimensional average magnetic field strengths for the inner part of the disc

$\lg E_M$	$\langle B\rangle_{\rm disc}$ [μG]
-2.5	1.0
-2.0	1.8
-1.5	3.2
-1.0	5.6
-0.5	10.0

Comparing the intensity contours of observed and theoretical polarisation maps might provide rather stringent constraints on the value of the coefficient α_B in galaxies. For NGC 891 the outermost contour at $\varpi \approx 8$ kpc and $z = 0$ with a $I = 150\,\mu$Jy/beam corresponds to $I = 2\,10^4$ Jy/sr. With $k = 1$ (in Eq. (9)) the theoretical intensity at a similar position is in our model about $0.02 \times 5\,10^4$ Jy/sr, which is about twenty

times smaller than the observed value at $\varpi = 10\,\mathrm{kpc}$. By taking $k = 0.5$, which is well within the range of uncertainty, the theoretical value becomes close to those observed, because of the high power of B occurring in Eq. (15). The variations of the spectral index with position in the galaxy (Hummel et al. 1991a) will also have a significant effect on the theoretical intensity distribution. In addition, it is perhaps also possible that the observations overestimate the intensity if the field is highly intermittent and the filling factor small. Finally, we should remember that we have omitted the small scale magnetic fields.

It is interesting to note that although mean field dynamos have met difficulties when modelling the detailed solar magnetic cycle, they seem to be able to reproduce quite diverse galactic magnetic field structures rather more readily. Even allowing that we have detailed temporal data on the solar cycle, as opposed to "snapshots" of a number of galactic magnetic fields, we feel this is some evidence in favour of the basic validity of the mean field concept. One basic difference between solar and galactic dynamo models is that we have reasonably secure knowledge of galactic differential rotation, that can be inserted into kinematic dynamo models, whereas a satisfactory solar model must include a self-consistent calculation of large scale velocity fields. Thus it may be plausible to argue that difficulties in understanding the solar dynamo lie principally in the large scale dynamics. Another possibility is that the nature of the turbulence, as manifested in the parameterisation of the alpha effect and turbulent diffusivities, is rather different in the sun to the usually adopted concepts.

Acknowledgements. We thank R. Beck, G. Golla and S. S. Spencer for useful discussions. We are grateful to E. Hummel and S. Sukumar who provided polarisation maps shown in Figs. 1 and 2. DS is grateful to "Lunokhod" Ltd for financial support.

References

Beck, R.: 1991, *Astron. Astrophys.* **251**, 15
Boulares, A., Cox, D. P.: 1990, *Astrophys. J.* **365**, 544
Brandenburg, A., Nordlund, Å, Pulkkinen, P., Stein, R. F. Tuominen, I.: 1990, *Astron. Astrophys.* **232**, 277
Brandenburg, A., Donner, K. J., Moss, D., Shukurov, A., Sokoloff, D. D., Tuominen, I.: 1992, *Astron. Astrophys.* **259**, 453 (Paper I)
Breitschwerdt, D., McKenzie, J. F., Völk, H. J.: 1991, *Astron. Astrophys.* **245**, 79
Cioffi, D. F., Jones, T. W.: 1980, *Astron. J.* **85**, 368
Cordes, J. M., Weisberg, J. M., Frail, D. A., Spangler, S. R., Ryan, M.: 1991, *Nature* **354**, 121
Cox, D. P.: 1990, In *The Interstellar Medium in Galaxies* (ed. H. A. Thronson, Jr., J. M. Shull), Kluwer, Dordrecht p.181
Dettmar, R.-J.: 1990, *Astron. Astrophys.* **232**, L15
Donner, K. J., Brandenburg, A.: 1990a, In *Proc. Nordic-Baltic Astronomy Meeting* (ed. C.-I. Lagerkvist, D. Kiselman & M. Lindgren), Uppsala Univ. (Sweden), Astronomiska Observatoriet p.85
Donner, K. J., Brandenburg, A.: 1990b, *Astron. Astrophys.* **240**, 289
Elstner, D., Meinel, R., Beck, R.: 1992, *Astron. Astrophys. Suppl.* **94**, 587
Ferrière, K.: 1992, *Astrophys. J.* **391**, 188
Golla, G.: 1992, . PhD thesis, University of Bonn
Golla, G., Hummel, E.: 1992, *Astron. Astrophys.* (submitted)
Habe, A., Ikeuchi, S.: 1980, *Progr. Theor. Phys.* **64**, 1995
Hummel, E., Dettmar, R.-J.: 1990, *Astron. Astrophys.* **236**, 33
Hummel, E., Lesch, H., Wielebinski, R., Schlickeiser, R.: 1988, *Astron. Astrophys. Letters* **197**, L29
Hummel, E., Dahlem, M., van der Hulst, J. M., Sukumar, S.: 1991a, *Astron. Astrophys.* **246**, 10
Hummel, E., Beck, R., Dahlem, M.: 1991b, *Astron. Astrophys.* **248**, 23
Jennings, R., Brandenburg, A., Moss, D., Tuominen, I.: 1990, *Astron. Astrophys.* **230**, 463
Klein, U., Urbanik, M., Beck, R., Wielebinski, R.: 1983, *Astron. Astrophys.* **127**, 177
Ko, C. M., Dougherty, M. K., McKenzie, J. F.: 1991, *Astron. Astrophys.* **241**, 62
Krasheninnikova, Yu. S., Sokoloff, D. D., Ruzmaikin, A. A., Shukurov, A.: 1990, *Geophys. Astrophys. Fluid Dyn.* **50**, 131
Krause, F. 1967, Habilitationsschrift, University Jena
Krause, F., Rädler, K.-H.: 1980, *Mean-Field Magnetohydrodynamics and Dynamo Theory*. Akademie-Verlag, Berlin
Lang, K. R.: 1980, *Astrophysical Formulae*. Springer-Verlag, Berlin Heidelberg New York
Lockman, F. J., Gehman, C. S.: 1991, *Astrophys. J.* **382**, 182
Lockman, F. J., Hobbs, L. M., Shull, J. M.: 1986, *Astrophys. J.* **301**, 380
Meinel, R., Elstner, D., Rüdiger, G.: 1990, *Astron. Astrophys.* **236**, L33
Moss, D., Tuominen, I., Brandenburg, A.: 1990, *Astron. Astrophys.* **240**, 142
Poezd, A., Shukurov, A., Sokoloff, D.: 1992, *Monthly Notices Roy. Astron. Soc.* (submitted)
Rädler, K.-H.: 1986, *Astron. Nachr.* **307**, 89
Rädler, K.-H., Wiedemann, E.: 1989, *Geophys. Astrophys. Fluid Dyn.* **49**, 71
Rand, R. J., Kulkarni, S. R., Hester, J. J.: 1990, *Astrophys. J.* **352**, L1
Reynolds, R. J.: 1989, *Astrophys. J.* **339**, L29
Roberts, P. H., Soward, A. M.: 1975, *Astron. Nachr.* **296**, 49
Rüdiger, G.: 1990, *Geophys. Astrophys. Fluid Dyn.* **50**, 53
Rüdiger, G., Kichatinov, L. L.: 1993, *Astron. Astrophys.* (in press)
Rupen, M. P.: 1991, *Astron. J.* **102**, 48
Ruzmaikin, A. A., Shukurov, A., Sokoloff, D. D.: 1988, *Magnetic Fields of Galaxies*. Kluwer, Dordrecht
Sancisi, R., Allen, R. J.: 1979, *Astron. Astrophys.* **74**, 73
Sokoloff, D. D., Shukurov, A. M.: 1990, *Nature* **347**, 51
Sukumar, S., Allen, R. J.: 1991, *Astrophys. J.* **382**, 100
Sukumar, S., Velusamy, T.: 1985, *Monthly Notices Roy. Astron. Soc.* **212**, 367
Vainshtein, S. I. & Zeldovich, Ya. B.: 1972, *Sov. Phys. Usp.* **15**, 159
Weisshaar, E.: 1982, *Geophys. Astrophys. Fluid Dyn.* **21**, 285
Weliachew, L., Sancisi, R., Guélin, M.: 1978, *Astron. Astrophys.* **65**, 37
Werner, W.: 1988, *Astron. Astrophys.* **201**, 1

This article was processed by the author using Springer-Verlag LaTeX A&A style file version 3.